Applied Materials Today 15 (2019) 280–285

Contents lists available at ScienceDirect

Applied Materials Today

journal homepage: www.elsevier.com/locate/apmt

Short communication

Materials from trees assembled by 3D printing – Wood tissue beyond nature limits

Kajsa Markstedt[a,b], Karl Håkansson[a,b,d], Guillermo Toriz[a,c], Paul Gatenholm[a,b,*]

[a] Wallenberg Wood Science Center at Chalmers University of Technology, 41296 Gothenburg, Sweden
[b] Department of Chemistry and Chemical Engineering, Chalmers University of Technology, 41296 Gothenburg, Sweden
[c] Department of Wood, Cellulose and Paper, University of Guadalajara, Tonalá,450110, Mexico
[d] RISE Bioeconomy, P.O. Box 5604, SE-114 86, Stockholm, Sweden

ARTICLE INFO

Article history:
Received 29 August 2018
Received in revised form 27 January 2019
Accepted 7 February 2019

Keywords:
3D printing
Cellulose nanofibrils
Hemicellulose
Honeycomb design
Biomimetic

ABSTRACT

Materials from trees have the potential to replace fossil based and other non-sustainable materials in everyday products, thus transforming the society back to a bioeconomy. This paper presents a 3D printing platform which mimics wood biogenesis for the assembly of wood biopolymers into wood-like hierarchical composites. The genome was substituted with G-code, the programming language which controls how the 3D printer assembles material. The rosette was replaced by the printer head for extrusion of cellulose. Instead of microtubules guiding the alignment of cellulose, the printing direction was guided by an *x*/*y* stage, thus mimicking the microfibril angle. The printed structures were locked by an enzymatic crosslinking reaction similar to what occurs in the cell wall upon lignification. Hierarchical structures characteristic for wood were designed and printed with control of density, swelling and directional strength. Accelerating the development of the 3D printing technology helps realize the circular bioeconomy where garments, packaging, furniture and entire houses are manufactured by 3D printing wood.

1. Main

The growth of a tree is a complex process where multiple biopolymers are assembled into the hierarchical composite known as wood with a remarkable combination of light weight and strength. The top down processing of solid wood for construction and the processing of disintegrated fibres into 2D materials such as paper, board, textiles and films, does not allow for fabrication of 3D products with control of design. While there exist multiple uses of wood in todays' society, wood is essentially formed by nature for nature. The formation of wood tissue is a complex process controlled by numerous genes, as well as exogenous and endogenous factors [1]. Mature wood primarily consists of dead cells, of which only the cell walls remain after complete autolysis of the cell contents [2,3]. The cell wall is composed of multiple layers differing in cellulose microfibril angle [4,5] and composition (Fig. 1a). The hierarchical structure of wood is a result of the in situ assembly covering the biosynthesis of biopolymers: from the alignment of cellulose microfibrils at the nanoscale to the ring formation visible to the eye (Fig. 1a). Within the tree rings, another typical design feature is revealed, namely the honeycomb structure of the cell walls, which contributes to the strength and light-weight of wood the density being influenced by cell wall thickness. Trees are perennial and adapt their properties to meet changing environmental conditions throughout their long life cycle. For example, in the formation of reaction wood the cell wall structure and composition are altered to meet external conditions. Wood formation can be manipulated, to a certain extent, by external stimuli, such as applying force. A unique example of controlling wood growth to achieve demanded properties and shapes, are chairs produced by Full Grown, UK (Fig. 1c, d). These chairs are a result of the bottom up fabrication of the tree. It is a slow process taking several years. In contrast, 3D printed cellulose chairs (Fig. 1e) can be manufactured in minutes [6] or in a few days if scaled up to full sized chairs. 3D printing provides the ability to process composite materials into hierarchical 3D objects [7–11] and is therefore a suitable technology for mimicking the structural features found in wood. However, fabrication of 3D shaped materials with controlled hierarchical structures based on wood biopolymers has not been broadly explored [12–16]. In this paper, 3D printing technology is used for layer-by-layer assembly of wood biopolymers into wood-like hierarchical structures as a platform for new applications inspired by

* Corresponding author.
E-mail address: paul.gatenholm@chalmers.se (P. Gatenholm).

https://doi.org/10.1016/j.apmt.2019.02.005
2352-9407/

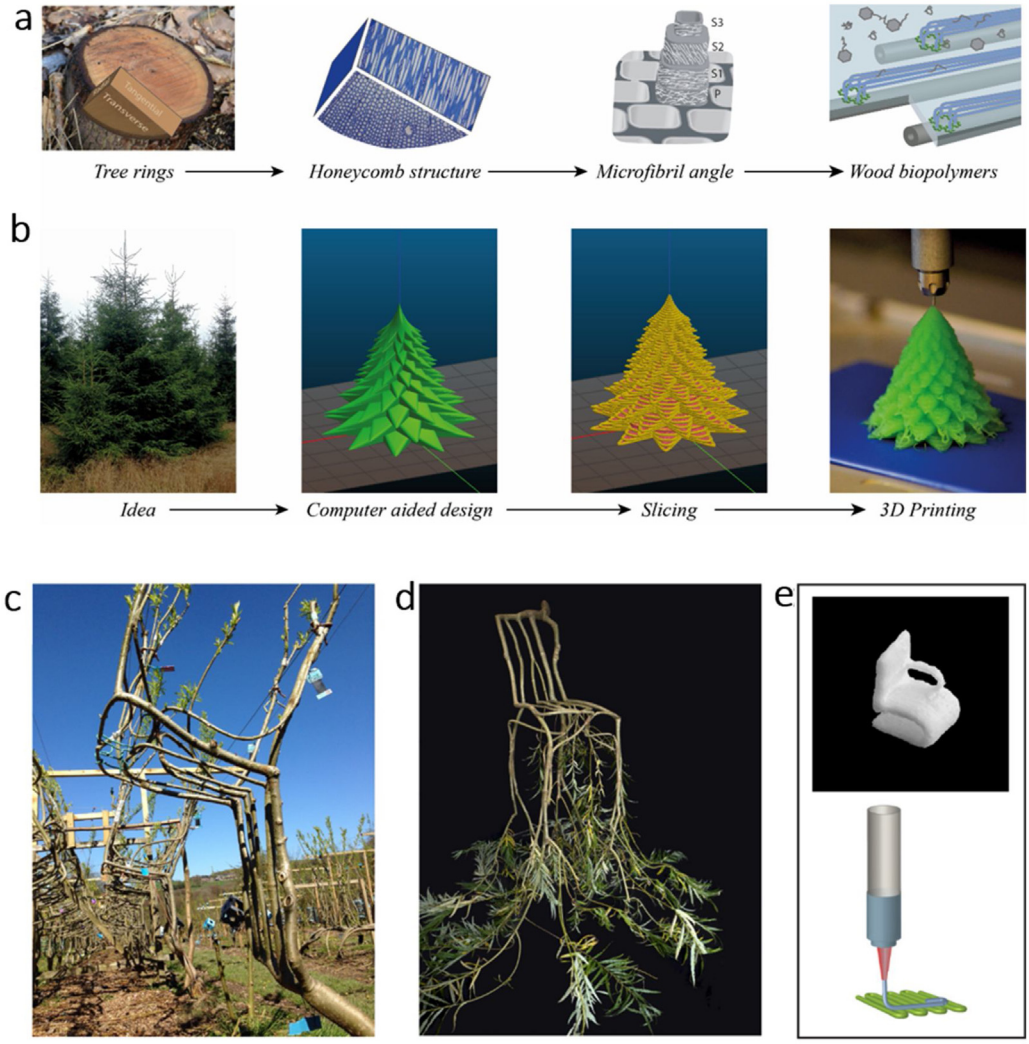

Fig. 1. Bottom up assembly in nature versus 3D printing. (a) Hierarchical structure of wood from the ring structure to the wood biopolymers (cellulose, hemicellulose and lignin) present in the cell wall. (b) 3D printing process from idea to printed object by computer aided design and slicing into layers for computer aided manufacturing. (c–e) Naturally assembled chair and 3D printed chair: (c) wood being grown into the shape of a chair. (d) Fully grown chair. (e) Chair which was 3D printed by extrusion of cellulose nanofibril based ink, an adapted image based on work presented by Ida Henriksson [6]. Image c and d have kindly been provided by Full Grown Ltd, UK.

wood tissue. The advantage of controlling composition, mechanical properties and swelling ability by bottom-up fabrication with wood based materials is demonstrated by 3D printing with wood-based inks composed of cellulose nanofibrils and crosslinkable hemicellulose.

Cellulose nanofibril hydrogels, CNF, processed from wood pulp, have proved to be very successful as inks in extrusion-based 3D printing [6,17,18] due to their suitable rheological properties [19,20]. The honeycomb features of wood were mimicked by 3D printing with CNF. In comparison to many other hydrogels used for extrusion-based 3D printing, the high viscosity of CNF dispersions (2–4 wt%) together with shear thinning enables 3D printing without support material [21] and instant crosslinking. Fig. 2a shows native wood tissue (*Picea abies*) where the red borders are the cell walls. The white centre is the lumen. The compound middle lamella, CML, which includes the primary cell wall and the middle lamella, is visible in the junctions of the honeycomb pattern. Fig. 2c shows the corresponding honeycomb structure printed with two CNF inks, white and red (coloured by food colouring), the secondary cell wall represented by the red ink and the CML represented in white. In contrast to wood tissue, where the cell wall thickness depends on the growing season, 3D printing controls the thickness, and consequently the density, independently of external factors. The honeycomb design was also used as a template for new designs, as in Fig. 2d where it forms the word WOOD.

Within the wood cell wall, cellulose microfibrils are aligned at different angles, called microfibril angle (MFA), with regard to the cell axis in the three layers of the secondary cell wall, S1, S2 and S3. S2 has a low MFA (4°–30°) providing strength and stiffness to the cell wall [1]. S1 and S3 are less rigid due to their higher MFA (60°–90°) [1]. The MFA is determined during cell wall formation when cellulose is synthesized and extruded as cellulose microfibrils by cellulose synthase complexes, CSCs, in the plasma membrane. The extrusion of cellulose generates a movement of the CSC where the direction and resulting MFA is controlled by microtubules.

In 3D printing, the CSC was replaced by a printing nozzle, which extrudes cellulose by applying pressure. Instead of microtubules, an *x*/*y*/*z* axis stage controlled the direction. 3D printing thereby shows great potential in adjusting the directional strength of composites by controlling the printing direction and design [8,22]. To demonstrate this, cylinders were printed at three different angles as a model of wood cells and their various MFA (Fig. 3a). 0° and 90° were achieved by printing layer by layer on a plate simply by rotating the cylinder design 90° and printing the cylinder either standing or laying down. However, when printing a cylinder with

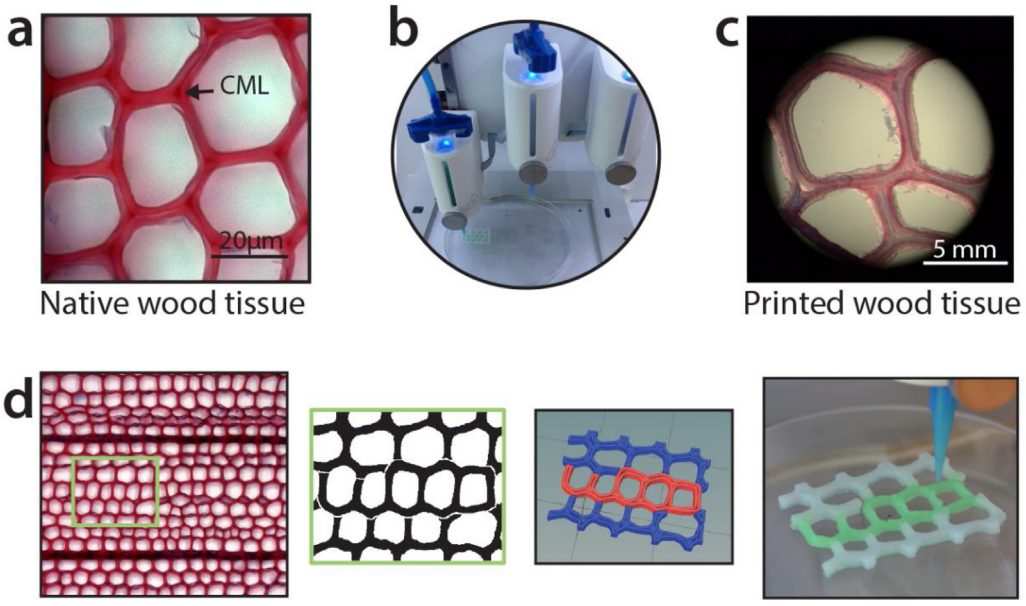

Fig. 2. Honeycomb structures. (a) Microscopy image of transverse sectioning of Norway spruce. (b) 3D printing with multimaterials using the 3D bioprinting BioX (Cellink). (c) Optical microscopy image of 3D printed wood tissue. The red ink represents the cell wall and the white ink represents the middle lamella. (d) 3D Printing of a modified honeycomb design to visualize WOOD within the honeycomb. The image shows the process from imaging of the honeycomb structure, image processing to STL format, and finally 3D printing. (For interpretation of the references to colour in this figure legend, the reader is referred to the web version of this article.)

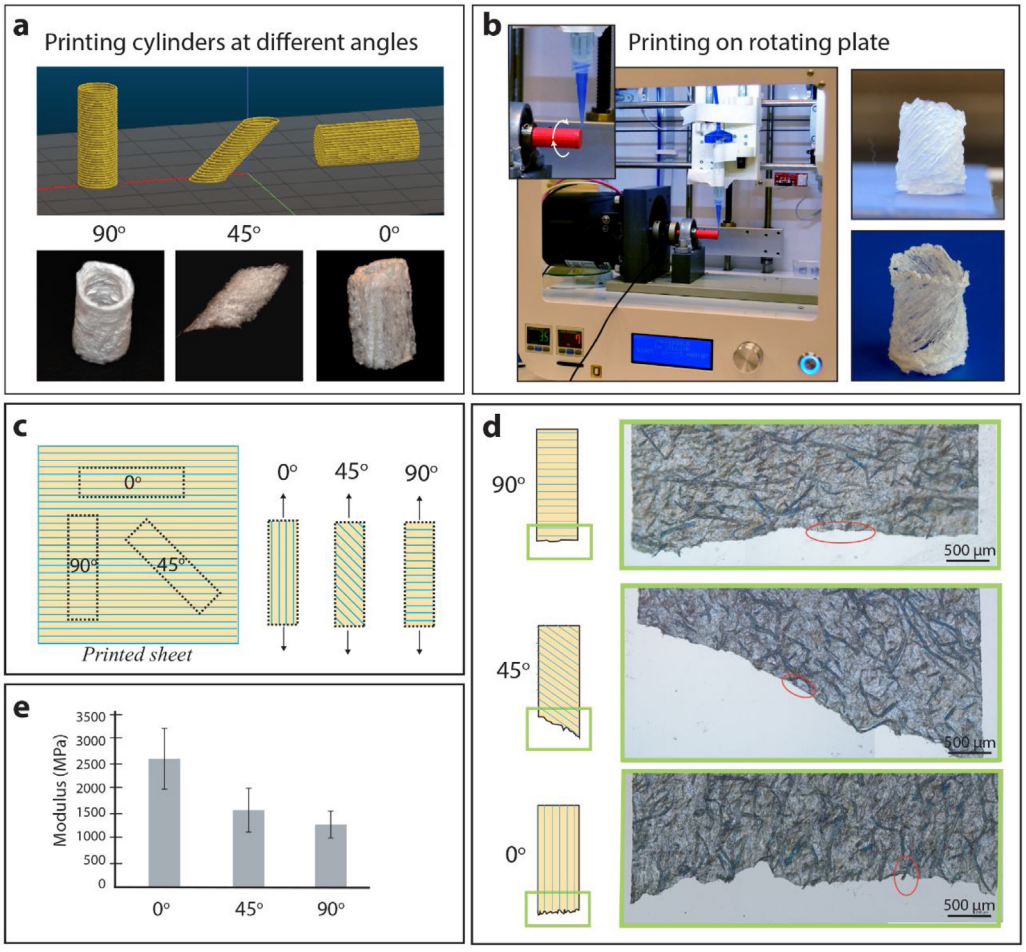

Fig. 3. 3D printing of specific printing angles. (a) Cylinders prepared printed at different angles (0°, 45°, 90°) showing the 3D designs in Slic3r software and the corresponding 3D printed cylinders. The cylinders have been freeze dried after printing with 3% CNF. (b) 3D printing at a 45° angle with a rotating plate. Photographs show the cylinder directly after printing (top) and after freeze drying (bottom). Tensile testing of films with different printing angles (0°, 45°, 90°). (c) Illustration of the printed sheet and the cut-out films. (d) optical microscopy images of the fracture surface for the films. The aggregates of fibrils correlate to the printed angle. The red circles mark the exhibited break: clean cut (top), rough cut (centre), pull out of fibres (bottom). (e) Modulus for the films with different printing angles.

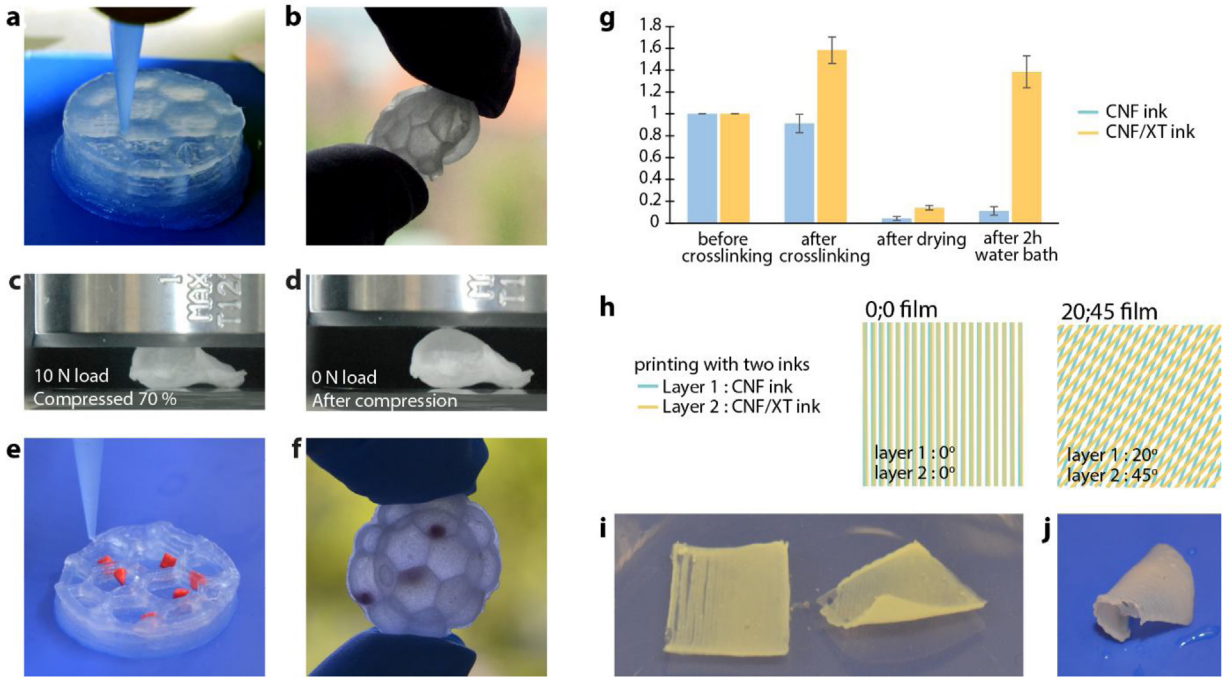

Fig. 4. Multifunctional 3D printed wood derived materials. (a–f) 3D cellular structure with honeycomb design. (a) 3D printing CNF (2.2 wt% carboxymethylated CNF) of cylinder (400 μm high, 2.5 mm diameter) with hollow pillars of honeycomb design. (b) Dried honeycomb cylinder: air captured in the printed structure resulting in a CNF bubble. (c and d) CNF bubble being (a) compressed to 70% of its height under a load of 10 N and (d) expanding back to original height of 7.8 mm. (e) Addition of solid particles while 3D printing honeycomb cylinder for encapsulation in CNF bubble. (f) Dried honeycomb cylinder with solid particles in separate honeycomb compartments. (g–i) Printing with multiple inks, CNF ink and CNF/XT ink, with different swelling capabilities. (g) Plot of change in mass of CNF ink and CNF/XT ink upon crosslinking, drying and reswelling in water bath. All values are normalized to the initial mass before crosslinking. (h) Printed designs for two inks with varying printing angle in each layer. In 0;0 film both layers are printed with 0 degree. In 20;45 film, layer 1 is printed at 20 degrees and layer 2 at 45 degrees. (i) Printed films in water bath. After printing and drying in air for 24 h. 0;0 film (left) shows no movement. 20;45 film folds (right) and keeps its folded shape when lifted out of the water bath (j).

45° inclination, 45° was only achieved on two sides of the cylinder. In wood, the MFA is helical, and the angle is present on all sides of the cell. To achieve this, cellulose was printed on a rotating plate (Fig. 3b).

Although the resolution of extrusion-based 3D printing is currently too low for printing at the scales present in wood, the printing process still influenced the mechanical properties at a macroscopic scale. This was confirmed by tensile testing of dried cellulose films with different printing angles (Fig. 3c). The highest modulus, 2600 ± 600 MPa, was measured for films with 0° printing angle (Fig. 3e). At 90° the modulus decreased roughly 50% resulting in a modulus of 1300 ± 270 MPa. Optical microscopy images of the fracture also displayed the influence of printing direction (Fig. 3d). At 0° the cellulose aggregates are pulled out, whereas 90° gives a cleaner cut. The modulus of samples printed at 45° was 1600 ± 400 MPa and their tendency to break at an angle reflected the printing direction. The films were strongest along the printed lines and weakest between the printed lines. This was expected since the thickness and amount of material ought to be lowest in the point between two lines. Also the tendency of cellulose aggregates to align along the printing direction provided strength to the films in the printing direction. Researchers have discussed the possibility of aligning particles at a nanoscale when 3D printing composites [7,8] and trends of alignment have been seen for inks of cellulose nanocrystals (CNC) [23,24]. Due to CNCs lower aspect ratio, they are not as entangled and align more easily than CNF. Both shear and elongation forces could help align CNF. Aggregates of CNF are visual in polarized optical microscopy images, where the shift in colour upon turning the polarization filter 90° showed that the alignment of aggregates is affected by the printing direction (Supplemental Data Figure S3). This is a beginning towards controlling the mechanical properties of a wood based material by 3D printing. This is an advantage to casting which often results in isotropic materials. 3D printing enables manufacturing of structures which utilize the materials anisotropic properties such as directional strength and swelling. Further studies on the influence of concentration, flow rate and nozzle geometry will help enable alignment of cellulose nanofibrils by 3D printing.

The honeycomb design and the printing of cylinders were combined in a 3D cellular structure (Fig. 4a–f). A cylinder with a honeycomb design of hollow pillars was printed with a solid top and bottom layer respectively (Fig. 4a). Upon drying (48 h), air was entrapped in the honeycomb cylinder and a strong and light-weight CNF bubble (density 0.12 g/cm^3) was formed (Fig. 4b). When compressing the bubble to 70% of its original height a load of 10 N was measured (Fig. 4c). After removal of the load, the bubble expanded back to its original height (Fig. 4d). Since cellulose has excellent oxygen barrier properties [25], the 3D printed cellular honeycomb structure is ideal for packaging oxygen sensitive substances i.e. for drug delivery and food. The compartments provided by the honeycomb pillars were retained after drying. Fig. 4e shows how solid particles were added in the honeycomb compartments while printing. After drying, the solid particles remain within their compartments thanks to the honeycomb walls (Fig. 4f). Thus, 3D printed CNF bubbles show promising features for advanced packaging with their cellular structure, separated compartments, light-weight and oxygen barrier properties.

The entangled network of CNF is not strong enough to form free-standing gels and the printed structures of CNF collapse if subjected to external forces. The concept of a composite is achieved by adding hemicellulose and lignin to the CNF inks. Hemicelluloses interact strongly both with cellulose and lignin and function as the glue of

the cell wall. In wood, lignin is polymerized from monolignols by enzymes. Lignification confers compression and bending strength to wood. Similarly, inks need to be crosslinked to obtain free-standing structures after 3D printing. We have recently shown that biomimetic cross-linkers of hemicellulose modified with tyramine (XT), a molecule analogue to lignin, can been used for 3D printing when mixed with CNF [26]. Figures S1 and S2 in supporting material shows that CNF mixed with XT, in addition to results presented in our previous work [26], has suitable properties for 3D printing. Thus, the rheological properties of CNF remain when mixed with XT. It is shear thinning once the yield stress is reached and has a high viscosity at low shear rates. In wood, the composition of biopolymers varies across the cell wall. Similarly, by 3D printing with multiple inks, the composition, such as varying amounts of hemicellulose in the ink, can be varied within the printed structure. Fig. 4h–j demonstrates this where a grid was printed with CNF/XT ink and CNF ink. The printed grid was dried flat and then submerged in a water bath. The difference in swelling between the two inks and thus the two layers, forces the printed grid to fold thereby enabling fabrication of soft actuators induced by changes in humidity. Fig. 4g shows how after drying and submersion in water, the weighed mass of CNF/XT ink is 1.4 times larger than the initial mass, before crosslinking while CNF ink does not even reach its initial mass due to hornification. The presence of XT in CNF/XT ink hinders hornification and allows for swelling in water after drying. Fig. 4i shows the importance of printing direction where movement only occurred for films with layers printed in different angles. When printing both layers with CNF ink, motion was not promoted, independent of printing angle, because of the very low swelling. Folding induced by humidity could be utilized in advanced wound dressings. The shape of the wound dressing would change upon contact with wound fluids to fit the convex and concave surfaces of the human body, thereby securing a conformal contact with the wound surface [27–29].

In summary, a platform has been established for 3D printing wood composite structures using wood biopolymers. The findings in this work can be employed in future applications of 3D printing with wood and other composite materials. Since wood is a composite, the 3D printing technology should, in addition to assembly of material into specific shapes, be utilized to design and print hierarchical structures where properties vary within the structure. The variations in the printed construct could be composition, fibril alignment or crosslinking density. With controlled design and fabrication, products with multifunctional properties could be achieved such as advanced wound dressings, smart textiles, packaging or soft robots.

2. Materials and methods

2.1. Materials

Cellulose nanofibril dispersions were kindly provided by Innventia (now RISE bioeconomy). Enzymatic pre-treated CNF was used for printing the honeycomb structures. The cylinders and films for tensile testing were printed with 3 wt% carboxymethylated CNF.

CNF/XT inks were prepared by mixing CNF with modified xylan, XT following the procedure of Markstedt et al. [26]. Briefly, 0.3 g of xylan modified with tyramine (degree of substitution = 19) was added to 2.65 g of CNF (3 wt%, enzymatically pre-treated) and mixed with a spatula until a creamy dispersion with no visible xylan particles was formed. Horse radish peroxidase (0.6 mg/ml) was added to the CNF/XT inks to assure uniform crosslinking upon addition of H_2O_2.

2.2. Swelling

The swelling ink (3 wt% carboxymethylated CNF) and CNF/XT ink were compared by weighing the change in mass upon crosslinking and reswelling after drying of CNF. Roughly 20 mg of CNF ink and CNF/XT ink was dispensed onto a petri dish and weighed ($n = 5$). The inks were then submerged in their respective crosslinking solutions, CNF ink in 0.1 M $CaCl_2$, and CNF/XT ink in 1 wt% H_2O_2 and the mass was weighed after 10 min. The samples were dried in air for 24 h. After weighing the dried samples, they were submerged in water for 2 h and their final mass was weighed. The mass weighed for all samples at all stages was normalized to the initial mass measured before addition of crosslinking solution.

2.3. Preparation of printing files

Cylinders were designed with the online software TinkerCad and exported in STL-format. STL files for printing of a tree were provided by thingiverse. STL files of the honeycomb structure of spruce sections were based on optical microscopy images of samples provided by Umeå Plant Science Centre. The microscopy images were processed in ImageJ software to receive a black and white image that was converted into STL by the online software SELVA (Sur3D).

STL files were then further processed by Slic3r software or Cellink Heartware (Cellink, Sweden) to generate G-codes for Inkredible and BioX, alternatively processed by STL software (RegenHu) to generate G-codes for 3D Discovery (RegenHu). Very simple designs (printed films) for printing with 3D discovery were designed and saved as G-code with BioCAD software (RegenHu).

2.4. Printing

Extrusion based printing with Pneumatic and microvalve dispensing printer heads was used for all inks. Three printers were utilized: RegenHu, Inkredible, BioX. The various printing designs were fabricated at printing speeds of 10 mm/min and 20 mm/min. For the pneumatic printer heads conical nozzles with an outlet diameter of either 250 μm or 400 μm were used. A straight nozzle with a 300 μm diameter was connected to the microvalve dispenser. The applied pressures varied from 8 kPa to 80 kPa depending on the yield stress of the inks and geometry of the printing nozzle. The printing height and distance between printed lines were adapted for each ink and nozzle geometry.

2.5. Microscopy

Images of printed honeycomb structures were taken by optical microscopy. 3D printed structures dried in air were studied in optical microscopy (Axio Scope A1, Carl Zeiss) in cross-polarized light mode to visualize the alignment of cellulose nanofibril aggregates.

2.6. Freeze drying

Printed cylinders were placed in a freeze at −40 °C followed by freeze drying (Heto PowerDry PL3000) for 24 h or until completely dry.

2.7. Tensile testing

The tensile strength of sheets with three different angles, defined as the printing direction with respect to the length of the film sample, were compared: 0°, 45° and 90°. The sheets were prepared by printing one layer of adjacent lines with carboxymethylated cellulose nanofibril dispersions, 3 wt%. After

printing, the sheets were dried at 70% humidity followed by equilibration at 50% relative humidity and 23 °C for a minimum of 24 h. After drying the mean thickness of the films was 15 μm. Rectangular films 10 mm × 3.64 mm were cut out at 0°, 45° and 90° angles with respect to the printing direction. Tensile tests were performed by a DMA Q800 of which the films were placed in the tensile clamp and tested at a strain rate of 2%/min. The modulus was calculated and averaged for 6 samples.

Author contribution

Experiments were conceived and designed by K.M., K.H. and P.G., and were conducted by K.M. The main paper was written by K.M. All authors have revised the paper and given approval to the final version of the manuscript.

Acknowledgements

The Knut and Alice Wallenberg Foundation is kindly acknowledged for financial support of this research in the framework of the Wallenberg Wood Science Center (WWSC).

Appendix A. Supplementary data

Supplementary data associated with this article can be found, in the online version, at doi:10.1016/j.apmt.2019.02.005.

References

[1] J. Fromm, Cellular Aspects of Wood Formation, 1st ed., Springer, New York, Berlin, 2013, pp. 20.
[2] C.L. Courtois Moreau, et al., Plant J. 58 (2) (2009) 260.
[3] H. Fukuda, Plant Mol. Biol. 44 (3) (2000) 245.
[4] B.R. Barnett, V.A. Bonham, Biol. Rev. 79 (2) (2004) 461.
[5] N. Gierlinger, et al., J. Exp. Bot. 61 (2) (2010) 587.
[6] K.M.O. Håkansson, et al., Adv. Mater. Technol. 1 (7) (2016) 1600096.
[7] D. Kokkinis, et al., Nat. Commun. 6 (2015) 8643.
[8] A.R. Studart, Angew. Chem. Int. Ed. 54 (11) (2015) 3400.
[9] T. Ahlfeld, et al., Biofabrication 9 (3) (2017) 034103.
[10] R. Cornock, et al., Biofabrication 6 (2) (2014) 025002.
[11] L.S. Dimas, et al., Adv. Funct. Mater. 23 (36) (2013) 4629.
[12] L.A. Berglund, T. Peijs, MRS Bull. 35 (3) (2010) 201.
[13] G. Fritz Popovski, et al., Adv. Funct. Mater. 23 (10) (2013) 1265.
[14] W. Kasai, T. Kondo, Macromol. Biosci. 4 (1) (2004) 17.
[15] K. Prakobna, et al., Comp. Part A: Appl. Sci. Manufact. 88 (2016) 116.
[16] T.T. Teeri, et al., Trends Biotechnol. 25 (7) (2007) 299.
[17] K. Markstedt, et al., Biomacromolecules 16 (5) (2015) 1489.
[18] J. Leppiniemi, et al., ACS Appl. Mater. Interfaces (2017).
[19] O. Nechyporchuk, et al., Carbohydr. Polym. 112 (0) (2014) 432.
[20] M. Paakko, et al., Biomacromolecules 8 (6) (2007) 1934.
[21] R. Suntornnond, et al., Int. J. Bioprint. 3 (1) (2017) 4.
[22] A. Le Duigou, et al., Mater. Des. 96 (2016) 106.
[23] G. Siqueira, et al., Adv. Funct. Mater. 27 (12) (2017) 1604619.
[24] A. Sydney Gladman, et al., Nat. Mater. 15 (4) (2016) 413.
[25] C. Aulin, et al., Cellulose 17 (3) (2010) 559.
[26] K. Markstedt, et al., ACS Appl. Mater. Interfaces 9 (46) (2017) 40878.
[27] B.C. Streifel, et al., Macromol. Biosci. 18 (5) (2018) 1700414.
[28] Z. Muwaffak, et al., Int. J. Pharm. 527 (1) (2017) 161.
[29] J. Leppiniemi, et al., ACS Appl. Mater. Interfaces 9 (26) (2017) 21959.